Invest to Save Budget

Improved Air Quality Forecasting
Invest to Save Report ISB52-10

Dispersion model testing using dual lidar data.

By

CG Collier, F Davies, AR Holt, DR Middleton, GN Pearson, DV Willetts & RI Young.

30 June 2004

Authorisation

Prepared by	Dr RI Young
Title	
Signature	
Date	June 2004
Location	QinetiQ Malvern

Principal authors	Dr GN Pearson
Appointment	QinetiQ Fellow, Remote Sensing
Location	QinetiQ
Principal authors	Professor DV Willetts
Appointment	QinetiQ Senior Fellow, Remote Sensing
	QinetiQ
Principal authors	Dr DR Middleton
Appointment	Air Quality Scientist
Location	Met Ofice, London
Principal authors	Dr F Davies
Appointment	Research Fellow, ISB-52
Location	Salford University
Principal authors	Professor A Holt
Appointment	Propagation and Remote Sensing Research group.
Location	Essex University
Principal authors	Dr RI Young
Appointment	Project Manger, Remote Sensing
Location	QinetiQ
Principal authors	Professor CG Collier
Appointment	Dean, Faculty of Science, Engineering and Environment
Location	Salford University
Principal authors	
Appointment	
Location	

Record of changes

Issue	Date	Detail of Changes
1.0	30 June 2004	First Release

EXECUTIVE SUMMARY

This report ISB52-10 was produced under Project 52 of the Invest to Save Budget, or ISB. The aim of this project is to improve atmospheric pollution dispersion models with the goal of improving air quality forecasting. During the project life, the team will be developing a better understanding of airflow near the earth's surface, focussing especially on urban meteorology. This will be achieved through the gathering of accurate 3-Dimensional wind flow data using laser radars, also called lidars, and by incorporating that new knowledge into the dispersion models.

A lidar is similar to conventional radar but uses an invisible, eye-safe, laser beam as its source of radiation. The great advantage of lidars for monitoring wind flow is that they can make more precise measurements than conventional radars and can probe to greater heights than most tall masts. In addition, lidars can make measurements in regions of the lower atmosphere above a city, which would be inaccessible to either aircraft or tethered balloons.

The lidars work by measuring the Doppler shift of light back-scattered from fine aerosol particles (water droplets, dust, etc) suspended within the atmosphere. The line of sight velocity component of the wind is then calculated. By sampling at different angles, and combining results from the two lidars, a picture of the three dimensional airflow in a scanned region can be assembled. Typically the scanned volume will be a few cubic km with the probes separated by up to 10 km.

This report describes the dispersion model data gathered for comparison to lidar observations. It tabulates results from the mesoscale/NAME model with the corresponding single and dual lidar data. Whilst the comparison between the dispersion model predictions and lidar observations is ongoing the initial results prove the usefulness of lidar in observing the nature of the evolution of the boundary layer across the rural urban interface. This is particularly prominent in that the height of the top of the boundary layer is clearly shown not to be constant and (at least for the samples examined) the spatial variations across the rural urban interface are more dynamic than previously thought.

List of contents

1. INTRODUCTION

Local air quality management uses dispersion models to forecast poor air quality events. Whilst there are a number of models in use they all consider similar parameters principally: the mixing height, stability, and turbulence. Measurements of these parameters over urban areas are not routinely available. This is because to ensure good exposure synoptic stations are often located at airports. When data is collected from instruments placed upon city centre buildings careful evaluation is necessary to mitigate any local effects. Validation of urban models is thus hampered by a lack of observational data sets. Given these limitations the ISB-52 project has been investigating the application of remote sensing by scanning pulsed Doppler lidar for urban dispersion studies.

Two lidar systems have been developed and built by QinetiQ, Malvern. The development of the first lidar system (the Salford University lidar) was conducted under a previous contract, but the development of an identical second lidar system (the QinetiQ lidar) was conducted under the first phase of this project. The two systems have then been deployed on a summer and winter trial. This is the first time that two identical lidar systems have been used to make simultaneous measurements of the wind field. The use of two lidar systems has enabled the independent measurement of two components of the wind flow simultaneously on a second by second basis. Now a complementary set of dispersion model data has been collected and the process of comparing the lidar data to numerical predictions begun.

This report begins with a review of the lidars, their use on the ISB-52 trials and from those trials the nature of the data gathered. There is then a brief description of dispersion models with the emphasis being placed upon the NAME model because that is the main model used by the Project Team. Reviewing previous ISB-52 work gives an appreciation of the underpinning complexity in comparing the two data sets, a comparison which begins in section 4. Examples of this comparison process are shown before some early conclusions are drawn on where the lidar observations are likely to make an impact on improving air quality forecasts.

Finally in the appendix the mathematical derivation is given of how unambiguous wind flow data can be derived form the combination of dual lidar data.

2. DESCRIPTION OF LIDAR OBSERVATIONS

2.1 Equipment description

The two lidar systems have identical key features. Their operating wavelength is 10.6 μm with a range resolution of 112 m. Other system characteristics are detailed in table 1 of report ISB52-04. The minimum ranges of the systems are determined by the back reflections of the individual optical components within the lidar. The maximum ranges are dependent upon the alignment of components within the system and the aerosol loading of the atmosphere. The two lidar systems consequently show slightly different minimum and maximum ranges, due to their different alignments. These maxima and minima vary under different atmospheric conditions. The minimum and maximum ranges are approximately 700 m and 9000 m.

The basic set-up of the two systems was detailed in report ISB52-02. The design involves a TEA (Tranverse Excitation Atmospheric) laser along with two CW (continuous wave) lasers. One CW laser and the TEA laser are used to provide the atmospheric pulsed laser signal whilst the other CW laser is used as a reference signal for the heterodyne detection of the returning atmospheric signal. The pulse repetition frequency (PRF) of the two systems can be increased but the data acquisition rate is limited by the ability of the computer to keep up with signal processing.

The signal processing procedure is detailed in Pearson and Collier (1999) and uses a scheme based on correlogram accumulation with a discrete spectral peak estimator (Rye and Hardesty, 1993). Accumulation of the return signal is carried out to improve the estimate of the calculated Doppler velocity. The amount of accumulation can be varied and this along with the PRF are inputs to the system processing procedure. The processing is done in real time enabling the continuous monitoring of the system performance.

2.2 Winter trial description

The winter field trial was conducted in the vicinity of the QinetiQ base at Malvern, Worcestershire. The QinetiQ lidar was based permanently at the QinetiQ site. On the 17th March, the first day of the trial, the Salford lidar was also sited at the QinetiQ site, approximately 25 m from the QinetiQ lidar. On the 18th and 19th March the Salford lidar was moved to the Three Counties Show ground, which was approximately 3 km south of the QinetiQ site. The longitude and latitude of these sites is detailed in table 1.1 of report ISB52-05. The two sites (QinetiQ site and Three Counties show ground) were both approximately 1.5 km east of the ridge of the Malvern hills. The other details of the site are discussed in section 2 of ISB52-5.

Dual Doppler lidar data was collected on the 18th and 19th March using three different line-of-sight configurations. These are detailed in table 3.3 of report ISB52-05. Before the trial, on Tuesday 11 March 2003, high pressure was to the West of the British Isles; showery rain had passed the British Isles on the 12th; then high pressure was centred over Scotland on Thursday 13 March 2003 (first day of measuring) and the UK was mainly dry with broken cloud; the centre of the high was over the North Sea on Friday 14 March 2003 and the UK had a pleasant sunny day. On Saturday 15 and Sunday 16 March 2003 it was also largely dry & sunny; from Monday 17 to Wednesday 19 March 2003 to country was still under anti-cyclonic conditions, warm

and dry, with fog or some frosts at night. On Thursday 20 March 2003 there was a front over the Irish Sea up to S. Scotland. During the trial, excepting on the Sunday (when data were not taken) the weather was anti-cyclonic, and cloud cover slight and winds speed light and variable.

2.3 Summer trial description

The summer trial was carried out under very mixed meteorological conditions at RAF Northolt, Greater London. RAF Northolt is to the west of central London on the border between mostly rural countryside to the west, and more urbanised (residential) areas to the east. The Aerodrome enabled the two lidars to have a separation distance of approximately 1.6 km. The results from the summer urban field trial are discussed more fully in this paper.

The summer field trial was conducted between the 8th and 23rd July 2003. The meteorological conditions through this period were variable. During the first week of the trial the country was under anticyclonic, high pressure conditions. There was little cloud cover. The day and night time temperatures were abnormally high and the humidity was also extremely high. The winds were on average easterly. During the second week of the trial several thunderstorms with heavy rainfall occurred. This eventually stopped the trial. The trial restarted for the third week when weather conditions had settled into fairly typical low pressure, cloudy conditions with south-westerly winds and occasional showers.

The conditions in the first week of the trial were ideal for measuring the wind flow using lidar as there had been no rain for several days and the aerosol content in the boundary was very high. Consequently the high backscatter signal enabled the measurement of radial winds up to the maximum range of the system (9 km). During the second week of the trial the intermitted rainfall acted to clean the boundary layer air. The aerosol loading of the atmosphere was consequently quite low and the effective range of the system was reduced to 4 km.

Besides the twin lidar systems an automatic weather station and a single sonic anemometer, on a 2 m mast, were deployed. The mast height was dictated by the airport officials as the airfield was in full operational use. Met data was also provided by the UK Met Office in various forms, including local observations, from the Met Office operational mesoscale model (12 km resolution) and the NAME dispersion model.

2.4 Summary of data gathered and derived parameters

Report ISB52-03 section 2 identified the key parameters and consequently the required scan patterns needed for validation of the dispersion models. The conclusion was that the measurement of the height of the top of the planetary boundary was of top priority. Profiles of wind speed, wind direction and turbulence were also required. To achieve a set of observations representative of the statistics of pollution dispersal phenomena it was also recommended to dwell along one line of site for at least ten minutes.

Three basic types of scan techniques can be used;

- VAD (or Azimuth) scan (which sweeps out an inverted cone at fixed elevation angle),

- RHI (or Elevation) scan (which sweeps a vertical semicircle or sector of a circle for a fixed azimuth),
- Fixed Beam (Stare) (which maintains a fixed elevation and fixed azimuth for a specified sampling period, say 10-15 minutes, long enough for reliable turbulence statistics).

A combined technique has been developed for this study:

- Dual Fixed Beam: Data from two Fixed Beams combined at their intersection point.

From this work a number of scan patterns were devised to unambiguously observe specific dispersion model parameters under different ambient conditions. That each of these scan patterns was optimum for observing a specific phenomena implies that the scan pattern would be limited for other observations. Recognising these limitations was a key lesson learnt during the Project, as were the strategies adopted to ameliorate these limitations during the trials.

This Project has shown that there was no single scan pattern that can derive all the dispersion model parameters. These specific scan patterns did not involve the PPI scans over large volumes of space necessary for the 3D flow visualisation displays. So whilst the developed code has an ability to display such data little was gathered.

It was also found that the limits on usable range combined with the relative slow scan speed of a lidar system became significant design constraints when planning the field scanning patterns.
The full complement of data that is available from this field trial is extensive and only a sample it discussed in this report.

Table 1 outlines the scanning techniques and the meteorological parameters obtained from the scan and the required duration of the scan.

Scan Technique	Measured Parameter	Derived Parameter	Required length of scan (minutes)*
Fixed Beam	Radial wind velocity profile, v_r Radial wind velocity variance profile, v'^2_r System estimation error	Energy dissipation rate , ε Integral length scale, L_i Integral time scale, T	15
Vertically pointing fixed beam	Vertical velocity profile, w Vertically velocity variance profile, w'^2	Temperature flux, w't' Sensible heat flux at the surface, H Convective velocity scaling	15

*time includes time needed for taking of noise files for data processing procedure

		, w*	
Dual Fixed beam$^{\otimes}$	Profiles of the two components of horizontal wind, u and v Profile of variances, u'^2 and v'^2	Energy dissipation rate , ⌈ Integral length scale, L_i Integral time scale, T	15
VAD (azimuth scan)	Wind speed profile, u Wind direction profile Back-scatter Intensity profile System offset	Boundary layer height	15
RHI (elevation scan)	Profiles of area averaged values for u, v and w Profiles of area averaged values for u'w' and v'w'	Friction velocity, u* Roughness length scale, z_0 Roughness displacement height, d (N.B. for these parameters measurements must be within the surface layer)	30

Table 1 Parameters measured and derived from the various scan strategies

Using the fixed lidar beam values for the kinetic energy dissipation rate, integral length scale can be derived from the power spectra (Gal-Chen *et al* 1992, Davies *et al* 2003). The integral timescale can be estimated from the velocity lag autocorrelation curve (Drobinski *et al* 2000).

From using a vertically pointing fixed beam the convective velocity scaling can be estimated (Mayor *et al* 1997). From this an estimate of the heat flux, w't' and sensible heat flux at the surface, H, can then be calculated (Gal-Chen et al 1992).

In conclusion ISB-52 developed a number of differing scan patterns, each optimised for a different observation either in terms of parameter to be derived or to reflect the stability of the ambient conditions. These different scan strategies yield differing data sets which in turn necessitates differing strategies for using the lidar data to estimate the dispersion model's parameters.

3 DISPERSION MODEL

3.1 NAME model

Whilst ISB-52 endeavours to be of use to all dispersion models, comparison of lidar data to model prediction dictates the use of at least one dispersion model. For this work the Met Office NAME model was used.

Air quality forecasting in the U.K. relies upon the Met Office's Lagrangian multi-particle random walk dispersion model, or NAME. Local air quality management to comply with the Environment Act 1995 also uses dispersion models, especially the ADMS and Airviro models, along with simpler screening models. A more complete description of all of these models is given in ISB52 MS1. There are a number of parameters that are common to such models, such as the mixing height, stability, and turbulence. Measurements of these parameters over urban areas are not routinely available; synoptic stations are often at airports to ensure good exposure, and instruments placed upon city centre buildings require careful evaluation for local effects. Validation of urban models is thus hampered by a lack of observational data sets.

The NAME model has been run on Mesoscale data to ensure the Project Team has access to results from the latest model versions for the principle dates of both trials at locations relevant to the trial. This data is at 12km resolution, extracted at hourly intervals for the grid point nearest to RAF Northtolt. Variables extracted are listed in Appendix 1. In addition the eddy diffusivity is calculated outside NAME following the same equations used within NAME and drawing on values in the model as extracted (e.g. for friction velocity). This gives NAME profiles for the trial area. NAME 'plume' source attribution plots have also been derived to show where air masses come/go from/to.

3.2 Representation of the Boundary Layer Depth in the NAME model.

It is well known that a dispersion model's performance is extremely sensitive to mixing layer height. For example if the estimate of the mixing layer height is too low then the forecast for poor air quality will be overly pessimistic. This is particularly important for modelling traffic emissions which tend to peak in the morning and early evening, times of transition when proper mixing height and stability diagnosis is most affected by urban factors. How the NAME model calculates boundary layer height is described below.

The calculation of the boundary layer begins with Numerical Weather Prediction (NWP) data (fields-files) being inputted into NAME from the Met Office Unified Model; these files include wind speed u, potential temperature θ, etc. at many vertical levels z at every grid-point. The correct magnitude of boundary layer depth is crucial for modelling the advection, dispersion and deposition to the ground, as reported by Maryon et al. (1999). They explained that at the time NAME was first developed, the sensitivity of the modelling to boundary layer depth was somewhat unexpected. It remains a reason for the importance assigned to establishing boundary layer depth in this urban lidar project.

NAME can use the NWP boundary layer depth as calculated by the weather forecast model. This has a numerical value defined at each grid-point. Alternatively, NAME uses NWP data to derive boundary layer depth in two ways (MS6).

The critical Richardson Number method and parcel ascent method are both calculated in NAME, then the larger of the two boundary layer heights is selected. If the result is small, then it is reset to the minimum value, typically 80 metres:

- The Richardson Number method, which relies upon wind speed and potential temperature profiles, is adopted mostly at night (stable conditions).
- The parcel ascent method, which relies solely upon the potential temperature profile, is mostly adopted in daytime (unstable conditions).

However the exact selection depends upon the temperature and wind speed profiles that are received from the NWP model. Neither method is "aware" of whether it is day or night.

4 COMPARISON OF LIDAR OBSERVATIONS AND DERIVED PARAMETERS TO NWP PREDICTIONS

4.1 Factors that impact on relating Lidar Data to Dispersion Model Parameters

The parameters used in dispersion models such as NAME were tabulated and compared against the possible parameters calculated from lidar data. The key issue was how to use data from a single or a dual lidar experiment in order to calculate dispersion parameters. Several issues arose:

1. The lidar are volume average measurements. The dimensions of each volume are defined by the diameter of the beam (0.5 m at 9 km) and the range gate length (112 m).
2. Turbulence data such as a velocity variance are conventionally obtained on a sonic anemometer with three orthogonal components resolved directly at 4-20 Hz. The sonic anemometer is run for a period, means and fluctuations from the mean calculated; this requires measurements for a sustained period (say 10 minutes or more). The lidar yields a radial component along the beam at a rate of 0.2 Hz. Mean wind speed and direction are calculated from an area average azimuth (VAD) scan (Browning and Wexler). The VAD scan takes approximately 6 minutes.
   Dual lidar operation enables the measurement of two components of the wind flow simultaneously. From the two radial wind measurements, two orthogonal wind components can be calculated. It is possible to obtain the third orthogonal component of the flow through use of the continuity equation.

Bozier et al 2004 addressed the issue of different sampling rates and volumes to show that average wind profiles from sonic and lidar data compare well.

In the light of these factors, a list of dispersion parameters was prepared (ISB52-01 Table 3; ISB52-04 Table 5a in Section 9; ISB52-06 Table on p. 6 in Section 5.) that we felt might be measurable either by single or by dual lidar operation. This is presented in the next section.

4.2 Dispersion Model Parameters from lidar

As previously discussed the primary aim of the trial was to ascertain how lidar data could be processed to yield products which could be used to improve the forecasting of urban air quality by dispersion models. To this aim a list was drawn up to compare parameters that were used within the dispersion models to what could be obtained from a dual Doppler lidar trial. Table 2 summarizes the data products that were deemed to be useful and attainable using lidar data.

Variable	Symbol	NAME Perspective	Lidar Perspective
Boundary Layer Depth	h	Rural h value via UM NWP profiles. City has internal layer(s).	Strength of back-scatter signal identifies aerosol layer(s). (Menut et al 1999)
Mean flow velocity (space or time	$\overline{u}, \overline{v}, \overline{w}$	NAME uses 3-D fields (UM NWP) of $\overline{u}, \overline{v}, \overline{w}$ updated each time-step.	VAD data yields mean $\overline{u}$ and $\overline{v}$. $\overline{w}$ from vertical beam.

average)			
Turbulence	σ_u, σ_v, σ_w	NAME uses standard deviations of wind velocity component fluctuations σ_u, σ_v, σ_w.	Dual lidar data can provide fluctuations u', v', w' to obtain σ_u, σ_v, σ_w. .
Local friction velocity derived from local Reynolds stress	u_* $\overline{u'w'}, \overline{v'w'}$	NAME calculates u_* or uses UM NWP output for σ_u, σ_v, σ_w .	Dual lidar processing can yield Reynolds stress $\overline{u'w'}$, $\overline{v'w'}$ and friction velocity u_*
Log law for surface layer <u>mean</u> wind speed in neutral conditions	$\bar{u} = \frac{u_*}{k}\ln\left(\frac{z-d}{z_0}\right)$ Notation: Use d or z_d	NAME follows UM NWP log law. NAME has surface momentum roughness length $z_0(x,y)$ from database.	Dual lidar data for $\overline{u(z)}$ to verify profiles and check u_*, k, z_0, d .
Urban roughness sub-scale height	z_* z_* is height to which roughness affects turbulence statistics or	Name may be extended to use z_* if urban roughness sub-layer confirmed.	Dual lidar data for Reynolds stress and friction velocity may shed light on the existence an urban roughness sub-layer
Eddy dissipation rate	ε	NAME calculates ε for turbulence and plume rise schemes.	Lidar fluctuations processed to generate spectrum and estimate ε
Lagrangian integral timescale and Integral length scale	$\tau_L = \int_0^\infty R(\tau)d\tau$ $L_i = \int_0^\infty R(s)ds$	NAME uses τ_L in plume rise and turbulence schemes.	Decay time scales for auto correlation coefficient $R(\tau) = \frac{\overline{u'(t)u'(t+\tau)}}{\sigma_u^2}$ for lag τ , $R(s) = \frac{\overline{u'(x)u'(x+s)}}{\sigma_u^2}$ for lag s.
Sensible heat flux Flux of temperature fluctuation	H or Q $H = Q_H$ $= \rho C_p \overline{w'\theta'}$ $\overline{w'\theta'}$	Correct sign of H (and time transition) is very important for NAME.	Indirectly from lidar third moment $\overline{w'^3}$. (Gal-Chen et al 1992) Or from w_* as below.
Convective velocity scaling . Associated		Used in NAME for calculating turbulence,	From $\sigma_w^2 \approx \beta w_*^2$ (Angevine et al 1994) where $\beta \approx 0.4$ within $0.2 < z/h < 0.5$

with speed of convection (unstable).	$w_* = \left[hg \frac{\left(\overline{w'\theta'}\right)}{\theta} \right]^{\frac{1}{3}}$	as $w_* = u_* \left[\frac{z_i}{k\lvert L \rvert} \right]^{\frac{1}{3}}$	

Table 2. Matching of dispersion model variables to lidar observations

So far as the Project Team is aware, no group has previously tried compile such a list of dispersion model variables that are in principle amenable to lidar observation prior to a measurement campaign. In the remainder of this report the Project Team compare the parameters from our lidar results with the mesoscale/NAME data sets.

4.3 Examples of vertical profile comparisons

The mean wind speed and direction can be obtained with lidar using a VAD or azimuth scan (Browning and Wexler). The lidar is scanned at a particular elevation angle describing an inverted cone shape. Data at a particular range gate is then plotted and a sine curve is fitted. The phase of the curve gives the direction of the maximum wind speed and the magnitude of the curve gives the wind speed. The wind speed and direction obtained are therefore area averaged over the area described by the scan at that particular range. Figure 4.3.1 and 4.3.3 show the mean wind speed and direction from a series of VADs from 07:45 UTC to 08:48 UTC on the 16th July 2003. This data was taken as a thunderstorm was approaching and the wind field is seen to change considerably over this time period. Figures 4.3.2 and 4.3.4 show NWP model wind speed and direction profiles for 06:00 UTC and 09:00 UTC.

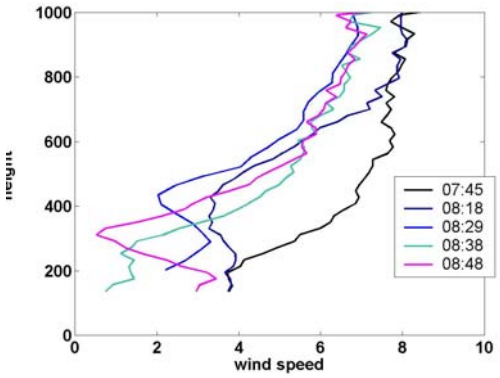

Figure 4.3.1 Mean wind speed and direction from lidar observation at 07:45

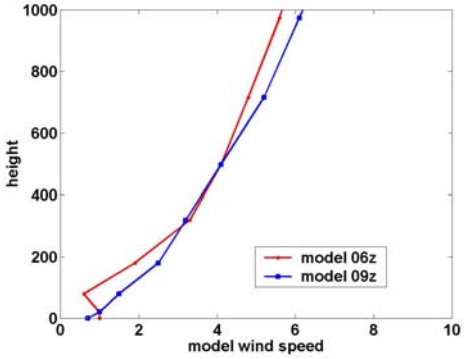

Figure 4.3.2 Mean wind speed and direction from NWP at 06:00

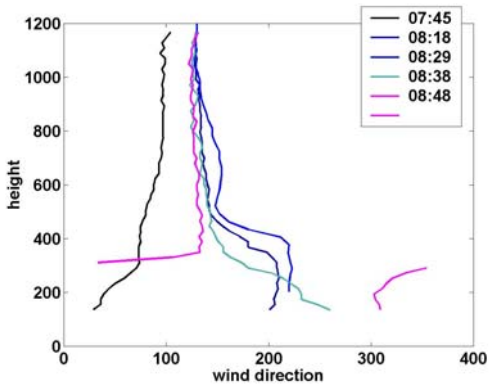

Figure 4.3.3 Mean wind speed and direction from lidar observation at 08:48

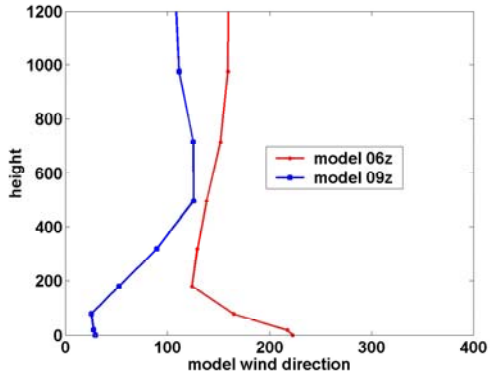

Figure 4.3.4 Mean wind speed and direction from lidar observation at 09:00

In this case the model profiles are comparable to the lidar data and correlate fairly well.

4.4 Turbulence Parameters

The aim of the dual Doppler lidar trials was to use the two lidars in a coordinated manner to enable the measurement of two of the velocity components independently. To this aim a series of 'stare' data were taken with the lidars looking in the plane defined by the line joining the two lidars. The set up is shown in figure 4.4.1.

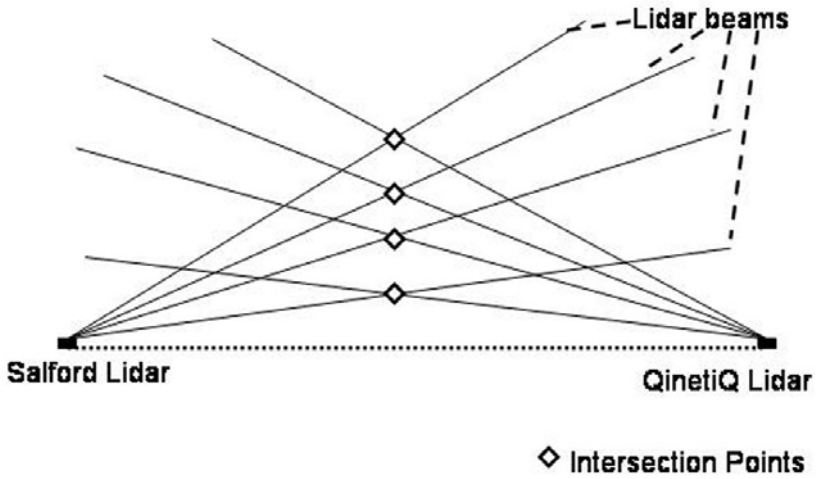

Figure 4.4.1. Schematic of dual Doppler Lidar scan

The data was taken from 11:30 to 12:30 UTC on the 23rd July 2003. The mean wind direction was nearly perpendicular to the plane containing the two lidars. The radial wind measured by the two lidars thus has a horizontal, and vertical, *w*, component. The data from the two beams are transposed to produce time series of horizontal and vertical winds. Since the two lidar beams are along the same horizontal axis no measure of the wind direction change with height can be made using this method. Only the horizontal (along the axis of the beam) and the vertical components can be calculated. Appendix 2 explains how wind data are derived from dual lidar modus operandi.

Mean wind speed and direction data taken from a single VAD of the QinetiQ lidar data is shown in the table below. The lidar data was taken from 12:25 – 12:32 UTC and is compared to NAME model data from 12:00 UTC. (The wind data from NAME is output at hourly intervals).

Height (m)	Mean Wind Speed (ms-1)		Mean Wind Direction (deg from N)	
	lidar	model	lidar	model
100		6.7		186
200	8.94	7.4	208	190
400	9.72	8.7	207	199
709	9.85	12.0	210	219

Table 3 Comparison of wind speeds and bearing.

Table 4 compares mean winds and standard deviation of the winds as derived from the dual lidar data from the two lidar systems between 11:30 and 12:30 UTC. The horizontal winds are measured along the axis of the lidar beams i.e. at an angle of 118 degrees from North. The lidar beam axis is thus approximately 70 degrees to the mean wind. The model data in table 4 is all data gathered at a height of 10 m. Since the wind speed and direction can change considerably in the near surface layer there is no reason to expect there to be a good correlation between mean wind speed data at 10 m and in the boundary layer above.

Height (m)	Mean horizontal wind in direction of the lidar axis ($m\ s^{-1}$)		Mean vertical wind, $\overline{w}$ ($m\ s^{-1}$)		Standard deviation of wind in direction of the lidar axis ($m\ s^{-1}$)		Standard deviation of w ($m\ s^{-1}$)		Momentum flux ($10^{-2}\ m^2\ s^{-2}$)	
	lidar	model	lidar	model	lidar	model	lidar	model	lidar	model
100	-0.32		1.9		0.50		3.4		-0.28	
200	1.24	1.73	0.04	0.01	0.59	1.18	1.45	0.96	0.22	-0.3
400	0.47		-0.15		0.59		1.78		-0.17	
709	0.26		-0.72		1.24		1.66		-0.74	

Table 4 Comparison of mean winds and standard deviation of the winds.

Using the derived horizontal and vertical winds at the lowest lidar level (100 m) values for kinetic energy dissipation rate and Lagrangian time scale have been calculated. These are shown compared to NAME dispersion model values in the table below. The NAME parameters are again shown for a height of 10 m unless otherwise stated. In this comparison the boundary layer heights compare very well.

	Lidar	Model
Boundary Layer Height (m)	880	850
Kinetic energy dissipation rate ($10^{-3}\ m^2\ s^{-3}$)	20.5 (@100m)	7.8 (@100 m)
Lagrangian time scale for horizontal wind, (sec)	350	233
Lagrangian time scale for vertical wind, (sec)	300	150
Convective velocity scale, w_* ($m^2\ s^{-2}$)	5.38 @ 100 m 2.29 @ 200 m 2.81 @ 400 m 2.62 @ 709 m	1.51

Table 5. Comparison of kinetic energy dissipation rate and Lagrangian time scale

4.5 Observation of Boundary Layer Depth

The atmospheric boundary layer is a layer near the surface, exchanging heat, momentum and moisture between the earth and atmosphere. Pollutants are dispersed in this layer. Boundary layer depth or height (of the top of this layer) depends on the wind speed, the vertical gradient of temperature, and the presence of either strong convection or surface cooling. It varies from below 100m to a few km. It is often greatest in late afternoon, say 1km, and falls in rural areas to about 100m in the evening as the ground cools. At night in urban areas, it has a larger value than the rural case. It follows a diurnal cycle.

Since pollutants can be dispersed vertically, we also speak of the mixing layer. The mixing depth represents the height reached by pollutants after release from sources at ground-level. Upward dispersion is eventually limited by an inversion above the

mixing layer. Most dispersion models require an estimate of the mixing depth or boundary layer depth/height so that any effective limit on vertical spread can be modelled. The effect is most important when the depth is shallow, when low lying plumes may be trapped near to the ground, or elevated plumes might be unable to reach the ground. The depth may be input to the model, or calculated by routines within the model.

Since the boundary layer depth or inversion height effectively set an upper limit to the vertical mixing of pollutants, they are of great practical importance for dispersion models. In earlier ISB52 reports (report ISB52-01,03 & 04), the boundary layer depth was identified as the highest priority parameter to be determined during the lidar field trials, followed by the wind profile, urban-rural differences, and values of the various boundary layer parameters.

Other workers have measured boundary layer depths by several means, such as the height where turbulence diminishes, or heat flux diminishes, or there is a marked discontinuity in profiles of wind/temperature/moisture, or the height of strong back-returns in acoustic sounding, or from lidar using the aerosol back-scatter signal. However the top of the boundary layer is not easily subject to a unique definition; different methods may yield different values. In this study we are fortunate that the pulsed Doppler lidar can be used to monitor simultaneously both the turbulent fluctuations with height, and the aerosol back-scatter intensity. We may thus compare the decay in turbulent motions with the decay in (from aerosol scatters) signal intensity (from SNR). As shown in ISB52 MS6 it was found that the decay in signal to noise ratio (SNR), which is strongly dependent upon availability of the aerosol particulates acting as centres for scattering, can be employed to detect the top of the boundary layer. This is because we assume the aerosol is largely concentrated in the boundary layer, and there is much less back scatter above the layer.

However in practice complications can arise that makes the interpretation of the lidar data more difficult, this could be due to low clouds or conditions of low SNR. For the instances where the gradient change is not so well marked further analysis is being conducted to investigate this phenomena, ISB52-MS6.

1) Malvern Winter Trial

The upper two graphs of figure 4.5.1 were shown in an ISB-52 technical working paper Pearson (2003). They are shown again here in conjunction with the potential temperature graph below in order to enable the issue of defining the boundary layer depth to be discussed. The parameter of interest here is the height in the lower atmosphere up to which any sources at or near the surface will be mixed. This may correlate with various features of the lidar data but the aim is to find the most robust technique for assessing this height both in the daytime and at night. Since any sources will be confined to this layer it is important to try to obtain the most representative height.

The lidar data from which the bearing, wind speed and backscatter values were derived was acquired between 18:50 and 19:03 of the 18th March 03. The potential temperature graph shows data from the NAME model for 18:00 of the same day. The lidar data shows a reduction in the backscatter at approximately the same height as the wind field exhibits a change of direction and a change in speed. This height is about

750m. The potential temperature plot shows a change in gradient at a height of about 450m.

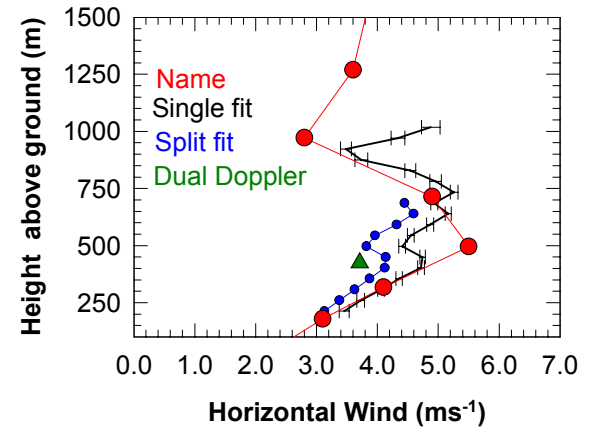

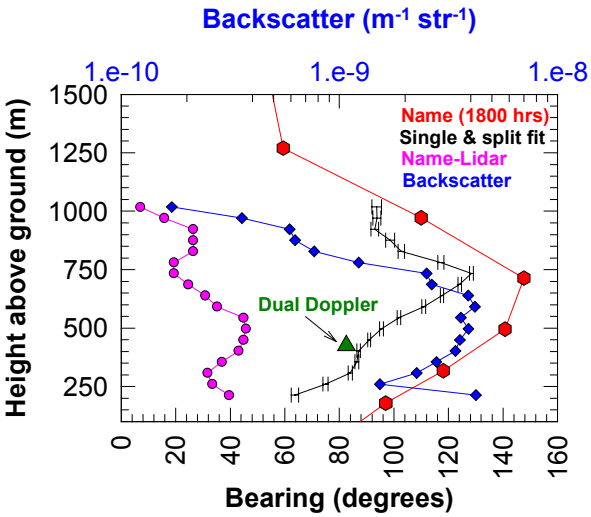

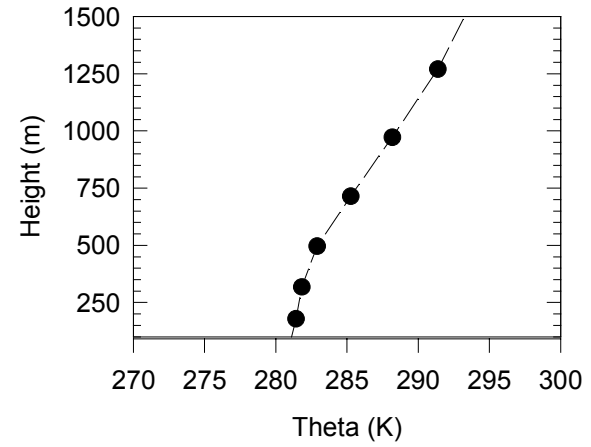

Figure 4.5.1 Top panel: The wind speed versus height as derived using two different VAD analyses (blue, black), dual Doppler (green) and the NAME model (red). Middle panel: The direction of the wind (VAD (black), dual Doppler (green) and NAME (red)) and the backscatter coefficient (blue) versus height. Bottom panel: The NAME potential temperature versus height.

The discrepancy in the bearing of the wind flow between model and observation is now ascribed to the impact of the close proximity of the Malvern Hills to the trial site. The nearest NAME grid point was several miles away and so did not account correctly for the local Malvern topology.

2) Example from the summer trial

As noted above the Boundary layer height can be inferred from lidar backscatter data. In high aerosol conditions and high pressure situations the boundary layer is usually capped by a strong inversion layer. Any aerosols within the boundary layer are effectively trapped. In such cases the height of the boundary layer can be inferred from lidar backscatter intensity data. Figure 4.4.2 shows data from 16:00 UTC on the 9th July 2003 probing the rural environment. The signal-to-noise (SNR) is plotted against height for the lidar data. A sudden decrease in the SNR is seen at approximately 1250 m above ground level.

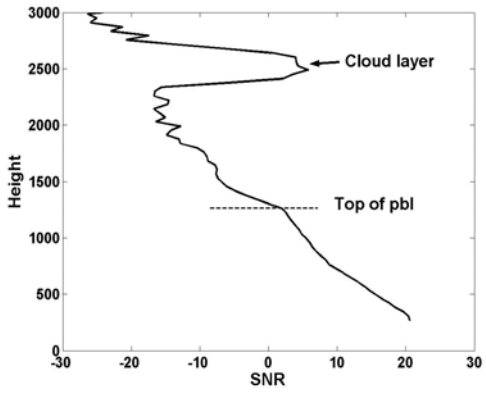

Figure 4.5.2 Lidar back scatter data from 16:00 UTC on the 9th July 2003

The sudden drop in SNR indicates the top of the boundary layer.

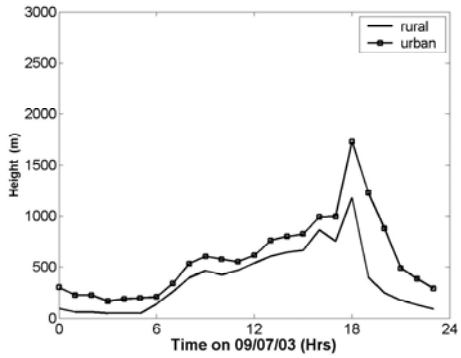

Figure 4.5.3 Boundary layer height over a 24 hour period from the ADMS dispersion model run under rural and urban conditions for the 9th July 2003.

Figure 4.5.3 shows model boundary layer height for urban and rural NWP model configurations. For the data on this day the boundary layer has its maximum height at 16:00 UTC. From comparison of the figures 4.5.2 and 4.5.3 it is concluded that the predicted boundary layer height is significantly lower than that observed by the lidar.

3) Horizontal and vertical variations of PBL

In the fine detail of the spatial variations of the top of the planetary boundary layer across the rural urban interface and the shape of the top of the PBL.

NAME is quite sensitive to the depth of the PBL. At present there is effectively no adjustment of the PBL in the model across the rural-urban interface. The lidar data have shown large variations (up to 1000m) across this interface on some occasions. Analysis of the synoptic situations / stability has revealed when these variations are largest.

At present the NAME model assumes that the top of the convective PBL remains uniform. The lidar data show that this is not necessarily the case, and the top may exhibit undulations. It is recommended that further investigation be undertaken to establish whether and how the NAME code should be modified to allow a non-uniform boundary top and rural to urban transition region. How this might be

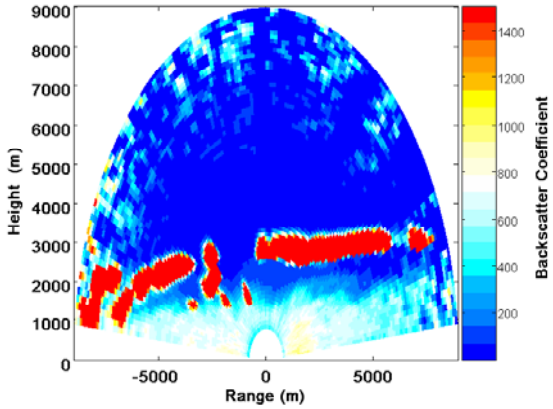

Figure 4.5.4. Elevation scan showing backscatter coefficient against height at 14:22 UTC on 9th July 2003. The scan has been carried out in an east – west plane. (i.e. positive ranges are due east of the lidar site).

approached depends upon the grid resolution of the mesoscale model data; as the grid approaches 1 km or less, such non-uniformity will be more explicitly represented. NAME would then reflect this.

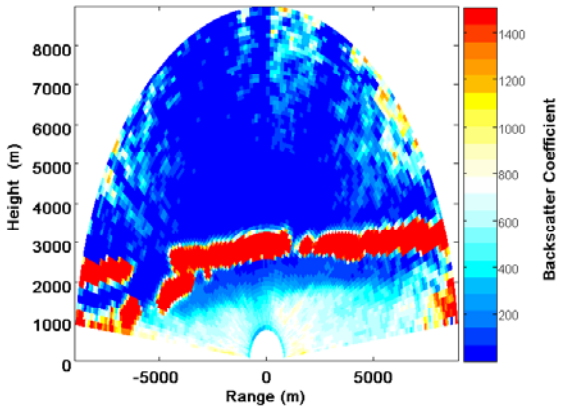

Figure 4.5.5. As figure 4.5.4, except at 14:35.

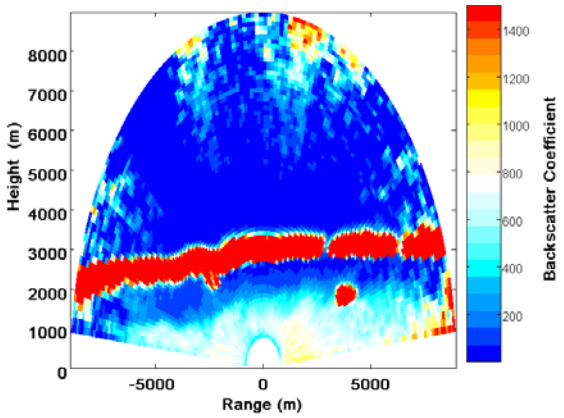

Figure 4.5.6. As figure 4.5.5, except at 15:01 UTC.

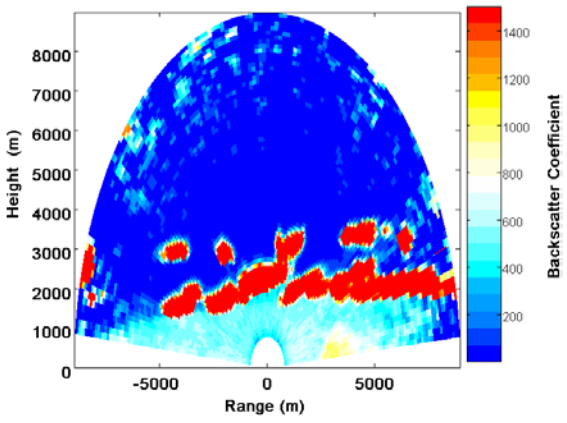

Figure 4.5.7. As figure 4.5.6, except at 16:50 UTC.

The series of figure 4.4.4 to 4.4.7 show 180 degree elevation scans from 14:22 to 16:50 UTC on the 9th July 2003. The figures show the backscatter coefficient plotted

against height. The red bands show very high backscatter values denoting cloud bands.

The scans have been taken in an east west direction, so that positive ranges denote distance east of the lidar position. The figures show there is a marked increase in the height of the cloud base above the 'urban' surface. In figure 5c an isolated cloud can however be seen lower in the atmosphere. An elevation scan, figure 6, shows that later in the day the lower cloud layer is more continuous.

It can also be seen in figures 4.5.4 to 4.5.7 that the pale blue contours of backscatter coefficient are higher over the 'urban' surface than over the more 'rural' surface. Estimation of the height of the mixing layer was carried out using the method of Mok and Rudowicz (2004) and showed that at approximately 15:30 UTC on the 9th July there was a difference of approximately 450m between the height over the 'urban' surface compared to the 'rural' surface. The distance between these two points was approximately 10km. This is considerably greater than the 200m height difference at 15:30 UTC as suggested by the different urban and rural ADMS model runs shown in figure 4.5.3.

4) 'Stand and stare' observation.

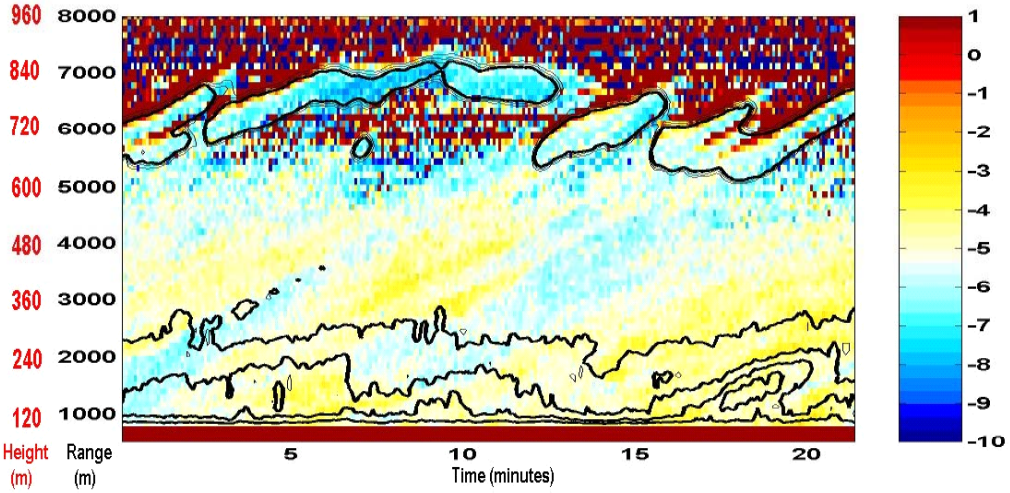

Figure 4.5.8 Result of a stand and stare observation

Figure 4.5.8 shows the results of a fixed stand and stare. This scan type enables a time dependent view of the flow field to be built up as the prevailing flow moves through the stationary inclined beam and convective cells rise through it. Colour coded radial velocity is plotted on successive inclined lines like a time series, with time on the horizontal axis and height on the vertical. Contours of intensity, or derived aerosol concentration, have been added.

At present the NAME model assumes that the top of the convective PBL remains flat. The lidar data shows that this is not the case, and the top often undulates. It is recommended that the NAME code should be modified to allow variability in the PBL height.

4.5 Relating Lidar Data to the Rural-Urban Transition

In measuring urban meteorology, long data runs are usually very hard to obtain. With complex and expensive lidar equipment, it is necessary to plan for a restricted number of trials. A striking feature of remote sensing is its ability to survey over significant distances. Here the maximum range could be up to 10-12 km, or down to 6 km, according to conditions. Having two lidars meant other scanning patterns designed to look at rural and urban conditions simultaneously could be used. Thus when running without beam intersection:

1. The beams can point in opposite directions, say into the approach flow over the rural south west, and with the urban flow to the north east.
2. The beams can be set orthogonal to each other, so one may be along the mean wind direction, the other cross wind.

Whilst this apparently negates a key advantage of having two similar instruments to measure unambiguously the flow field at a single point, it is apparent that observing over both the rural and urban surfaces simultaneously is an invaluable methodology for studying the rural-urban transition, and merits discussing at length. The ability to scan the beams and reach out several km is a clear advantage over fixed sonic anemometer measurements.

5. SUMMARY

Air quality forecasting in the U.K. relies upon the Met Office's Lagrangian multi-particle random walk dispersion model, or NAME. Local air quality management to comply with the Environment Act 1995 also uses dispersion models, especially the ADMS and Airviro models, along with simpler screening models. There are a number of parameters that are common to such models, such as the mixing height, stability, and turbulence. Measurements of these parameters over urban areas are not routinely available. This is because to ensure good exposure synoptic stations are often located at airports. When data is collected from instruments placed upon city centre buildings careful evaluation is necessary to mitigate any local effects. Validation of urban models is thus hampered by a lack of observational data sets. Given these limitations the ISB-52 project has been investigating the application of remote sensing by scanning pulsed Doppler lidar for urban dispersion studies.

ISB-52 has deployed twin lidars on two trials to gather pertinent observational data to support the further development of air quality models. The development of the lidars, their deployment and the results of their observations have been published in earlier ISB-52 reports. In this report dispersion model predictions have been derived for times and locations equivalent to the trials data and a comparison between the data sets begun.

Whilst the comparison between the dispersion model predictions and lidar observations is ongoing the initial results prove the usefulness of lidar in observing the nature of the evolution of the boundary layer across the rural urban interface. It is also marks a major achievement for the project. This is particularly prominent in that the height of the top of the boundary layer is clearly shown not to be constant and (at least for the samples examined) the spatial variations across the rural urban interface are more dynamic than previously thought.

Prior to this report, dispersion model parameter data measured in the UK for testing NAME have been restricted to mast data at an urban site (up to 45 m) in Birmingham, or rural data (up to 1 km) at Cardington. The Dual Doppler Lidars have been tested and shown to deliver useful results on these profiles especially at heights that conventional masts cannot reach (these are limited to 45 m in our experience) and also probing the atmosphere at significant horizontal distances from the instrument site in an arbitrary direction. Consequently the deployment of remote sensing means the findings of this report represent a significant advance in our understanding of the nature of the atmosphere across the rural urban interface. Further field trials are strongly recommended in order to build on this achievement.

As the Project's data are drawn together, a number of new scientific questions arise. These emerging questions will take significant effort to answer properly, an effort that goes beyond the scope of this current project. It is important to stress the fact that ultimately the lessons learnt from these comparisons of single and dual lidar with dispersion model parameters will lead to the improved understanding of the atmosphere. In turn this will allow the necessary adjustments of current models to make more accurate air quality forecasts in the future.

6 REFERENCES

[1] Matching urban lidar data to dispersion models. DR Middleton, ISB52-01March 02

[2] Boundary layer meteorology by pulsed lidar. Pearson, GN DV Willetts & RI Young. ISB52-02. April 02.

[3] Assessment of lidar performance and data from the first dual Doppler lidar trial. GN Pearson & DV Willetts ISB52 TWP March 2003.

4] Identification of key flow parameters for visualisation. RI Young, S Siemen, AR Holt & GJG Upton ISB52-03 Aug 02.

[5] Identification of key parameters for dispersion models. F Davies, C Collier, K Bozier & DR Middleton ISB52-04 Feb 2003

[6] The Determination of Kinematic Properties of a Wind Field using Doppler Radar. Browning and Wexler, Journal of Applied Meteorology, Vol. 7, 105-113pp, 1968

[7] Boundary Layer Measurements of Dispersion Model Parameters using Dual Doppler Lidar at Malvern, UK. F Davies, C Collier, A Holt, D Middleton, G Pearson, S Siemen, DV Willetts & RI Young. ISB52 -06 July 2003

[8] Description of the RAF Northolt ISB-52 Dual Doppler Lidar Trial. RI Young, GN Pearson, C Collier, F Davies & K Bozier. ISB52-07 August 2003

[9] Pearson G N and Collier C G (1999) A pulsed coherent CO2 lidar for boundary layer meteorology. *Q. J. R. Meteorol. Soc*., **125,** 2703 – 2721

[10] Gal-Chen T, Xu M and Eberhard W L (1992) Estimations of Atmospheric Boundary Layer Fluxes and Other Turbulence parameters from Doppler Lidar Data. *J.Geophys. Res*.**, 97** 18,409-18,423.

[11] Rye B J and Hardesty R M (1993) Discrete spectral peak estimation in incoherent backscatter heterodyne lidar. II Correlogram accumulation. *IEEE Trans. Geosci. Remote Sens*., **31**, 28 - 35.

[12] Maryon R H, Ryall D B and Malcolm A L (1999). The NAME 4 Dispersion Model:Science Documentation. Met Office Turbulence and Diffusion Note No. 262. Met Office London Rd Bracknell Berks RG12 2SZ, UK.

[13] Mok T.M. and Rudowicz C.Z. (2004) A lidar study of the atmospheric entrainment zone and mixed layer height over Hong Kong. *Atmospheric Research*, **69**, 147 – 163

[14] Bozier K.E. Pearson G.N. Davies F. and Collier C.G. (2004) Evaluating the precision of a transverse excitation atmospheric based CO2 Doppler lidar system with in-situ sensors. *J. Optics A: Pure Appl. Opt*. **6**, 1-9

7 GLOSSARY

ADMS	-	Atmospheric Dispersion Modelling System dispersion model from CERC
AEOLIUS	-	A dispersion model used by the Met office
AERMOD	-	A dispersion model from the American EPA.
BOXURB airflow	-	A dispersion model developed by the Met Office to describe through an urban canyon modelled as a box.
CW	-	Continuous wave
EPA	-	Environmental Protection Agency, a US government organisation
FWHH	-	Full width half height, a measure of the depth of field of the sensing zone of a CW lidar.
ISB	-	Invest to Save Budget
ISC	-	Dispersion model
LATAS	-	Laser Airborne True Airspeed sensor, an early Malvern Lidar
LDV	-	Laser Doppler Velocimeter
LDV1	-	Laser Doppler Velocimeter 1 (A Lidar developed at Malvern).
MRU	-	Met Office research unit
NAME	-	Main dispersion model used by the Met Office
NWP	-	Numerical weather prediction
RAM	-	A dispersion model
RHI	-	Range height indicator
TEA Dioxide	-	Transfer exited atmosphere (pressure). A type of Carbon lasers that emits pulses of relatively high energy. Used in the pulsed lidar to achieve measurements to greater ranges.

8 APPENDIX 1. OUTPUT DIAGNOSTICS FOR THE DISPERSION MODEL PARAMETERS IN THE NAME MODEL.

Introduction
The 'trajectory' run of NAME will out put the following array of dispersion model parameters, at the chosen height. Usually for most applications, the array at 10 m is sufficient.

Output Array Header
Trajectory Model Version 708
Mesoscale Met for Northolt
Run time: 13:03UTC 18/05/2004
Met data: Mesoscale
Met data

NORTHOLT
10m agl
0000UTC 08/07/2003

Table showing dispersion model parameters in the output columns.

NAME Parameter	**Description**	**Units**
Date	Date	dd/mm/yyyy
Time	Time, UTC	Hh:mn:ss
Longitude	Longitude, East >0, West <0	Decimal degrees
Latitude	Latitude, North >0, South <0	Decimal degrees
m agl	Chosen Height above ground level	m
m asl	Chosen Height above mean sea level	m
FL	Flight Level	100 feet above MSL
Pressure	Pressure at chosen height	hPa (mbar)
PMSL	Pressure at mean sea level	hPa (mbar)
P*	Pressure at the surface	hPa (mbar)
Wind spd	Wind speed at chosen height (10 m)	m s^{-1}
Wind dirn	Wind direction at chosen height (10 m) clockwise from North	degrees
Temp	Temperature at chosen height (10 m)	C
Sfc Temp	Surface temperature	C
Tot cld	Total cloud cover	fraction of 1 (8 oktas)
BL depth	Boundary layer depth (NAME parcel/Ri diagnosis)	m

Heat flx	Sensible heat flux (upwards >0)	W m^{-2}
U*	Friction velocity	m s^{-1}
W*	Convective velocity scale w_*	m s^{-1}
Vert Wind	Vertical wind speed w	m s^{-1}
RH	Relative humidity	%
Q	Specific Water Content	
Topog	Height of topography (as used in the Unified Model) above MSL	m
Z0	Roughness length z_0 for momentum	m
Dyn ppt	Dynamic precipitation rate	
Con ppt	Convective precipitation rate	
Con base	Height of convective cloud base	m
Con top	Height of convective cloud top	m
Con amnt	Convective cloud cover amount	fraction of 1 (8 oktas)
SigU (Hom)	Homogeneous Turbulence, Standard deviation of wind velocity fluctuations, σ_u (in NAME, $\sigma_u = \sigma_v$)	m s^{-1}
SigW (Hom)	Homogeneous Turbulence, Standard deviation of wind velocity fluctuations, σ_w	m s^{-1}
TauU (Hom)	Homogeneous Turbulence, Lagrangian integral time scale for horizontal fluctuations	
TauW (Hom)	Homogeneous Turbulence, Lagrangian integral time scale for vertical fluctuations	
KH (Hom)	Homogeneous Turbulence, eddy diffusivity for horizontal fluctuations	
KV (Hom)	Homogeneous Turbulence, eddy diffusivity for vertical fluctuations	
SigU (In)	Inhomogeneous Turbulence, Standard deviation of wind velocity fluctuations, σ_u (in NAME, $\sigma_u = \sigma_v$ to reflect importance of cross-wind fluctuations in dispersion)	
SigW (In)	Inhomogeneous Turbulence, Standard deviation of wind velocity fluctuations, σ_u (in NAME, $\sigma_u = \sigma_v$ as before)	
TauU (In)	Inhomogeneous Turbulence,	
TauW (In)	Inhomogeneous Turbulence,	
KH (In)	Inhomogeneous turbulence, eddy diffusivity in horizontal	
KV (In)	Inhomogeneous Turbulence, eddy	

	diffusivity in vertical	
SigUl	Limit on	
KHl	Limit on	
Rho	Density of air (Erroneous?)	kg m^{-3}
L	Monin Obukhov Length (Stability Parameter)	m
DTopog/dx	Incline of topography in x direction	
DTopog/Dy	Incline of topography in y direction	
DDzsum/Dx		
DDzsum/Dy		

Notes

Eddy Dissipation Rate ε (rate of decay of turbulent kinetic energy, with dimensions of kinetic energy per unit mass per unit time, or units $m^2 s^{-3}$) is not output from NAME as a diagnostic in these tables, but is calculable at some height z from the output values of u_*, L, z_i (BLD), and w_*, and these do not vary with height in the boundary layer of NAME, together with von Karman's constant κ=0.4 (dimensionless) according to:

Stable conditions, L>0.0,

Unstable conditions L<0.0,

Neutral conditions, L=0, the formulae above both reduce to the same result,

With the Homogeneous Turbulence scheme (a simpler, computationally faster scheme), NAME assumes typical average values of τ, σ and K are constant throughout the whole boundary layer. i.e. at a given position or grid point, they are allowed to vary with time of day, but not with the height z.

For the recently published Inhomogeneous Turbulence scheme developed by Helen Webster, NAME varies the values of τ, σ and K according to height within the boundary layer. i.e. they are allowed to vary with time of day, and with position, and are calculated explicitly using the height z.

9 APPENDIX 2 EXTRACTING WIND INFORMATION FROM SCANS USING TWO LIDARS

Introduction

A single lidar measures the component of the wind along the radial from the lidar. By performing a complete azimuth scan at constant elevation, it is possible to gain additional information. This is the VAD (velocity-azimuth-display) procedure. If the wind is constant over the coverage area of the scan, then the wind component measured will describe a sine wave when plotted against azimuth. Where the graph crosses the (azimuth) axis, the velocity is tangential to the radial at that azimuth. The direction of the maximum component gives the direction of the wind [cf figure 1]. The direction is often easier to obtain from the crossing point, than from the maximum.

Such a description is in general ideal, and other factors need to be taken into account. Firstly, there may be a bias in the lidar; this will be revealed as an offset in the sine curve. There will also be noise in the data, and this frequently occurs around the maxima/minima of the curve, making precise measurements of magnitude and direction difficult to obtain. It is also a fact that the VAD technique assumes that the component of the vertical velocity in the direction of the radial is negligible. This is a reasonable assumption at low elevations, but as the elevation increases, its validity decreases. Another factor to be considered is time. The lidar scans reasonably slowly, so that a complete azimuth scan typically takes 7-10 minutes. In conditions when the wind is changing rapidly, the wind at the beginning and end of the scan may differ significantly – changes of 6m/s have been observed. Consequently, the extraction of precise wind information from a single lidar can only be approximate, and relies on assumptions that may well not hold. It should be noted however that since the radius of the lidar scan will in practice be small (max 8km), the assumption of wind uniformity is probably normally valid.

The advantages of two lidars

With two lidars, one can measure two components of the wind. In dual-Doppler radar studies one can then invoke the continuity equation to obtain three equations for the three wind components, and thus obtain the total windfield. However, with current lidar technology, one cannot scan fast enough to obtain the volumetric scans needed. Moreover, if the study requires the time-series analysis of the velocity data, then a fixed stare on a given intersection volume is essential, and the continuity equation cannot be invoked. Consequently, only two equations exist and in general the windfield cannot be obtained without making assumptions. However, one component can be always be unambiguously derived, and in special cases, two components can be obtained unambiguously. These are now described.

1. Suppose A and B are the two lidars, situated at points with vector positions **a** and **b** respectively. Suppose that both lidars are sensing the wind at point P with vector position **p**. Let **PA** be the vector along PA (ie from P to A), **PB** be the vector along PB, and **AB** the vector along AB. Then **PA** + **AB** = **PB.** If V is the wind velocity vector, we measure $\mathbf{V}.\hat{\mathbf{p}}_{\mathbf{A}}$ and $\mathbf{V}.\hat{\mathbf{p}}_{\mathbf{B}}$. Hence the component of V along AB is given by

$$\mathbf{V.AB}/|\mathbf{AB}| = [\ \mathbf{V.PB} - \mathbf{V.PA}]/|\mathbf{AB}|$$

Hence The component of V along AB can always be obtained unambiguously.

2. Scans through vertical plane containing both lidars
We term this an "Along track scan" – the track being the line through the two lidars.
We assume the definitions in fig. 1.

Here $90° \geq \theta_A \geq -90°$
$90° \geq \theta_B \geq -90°$

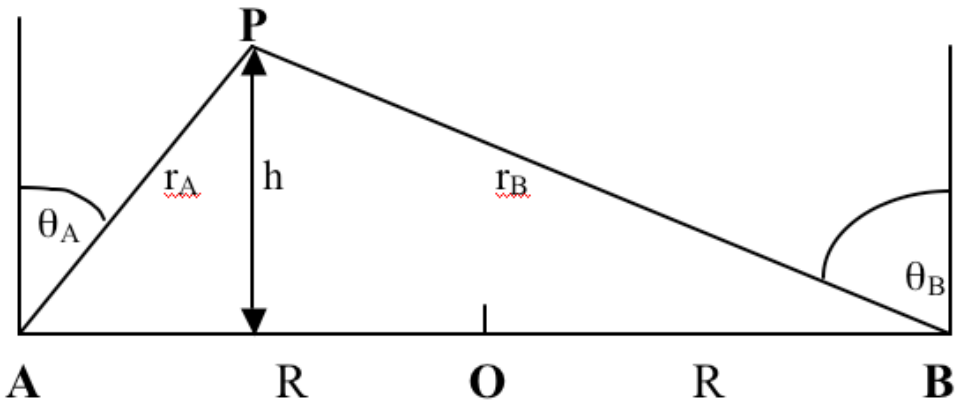

Figure 1

If h is the height of P
above AB

Then $r_A \sin\theta_A + r_B \sin\theta_B = 2R$

$$r_A \cos\theta_A = r_B \cos\theta_B = h$$

$$\Rightarrow \quad r_B = (r_A^2 - 4Rr_A \sin\theta_A + 4R^2)^{\frac{1}{2}}$$

Also $V_A = \mathbf{r}.\hat{\mathbf{p}}_\mathbf{A} = -V_{px} \sin\theta_A - V_{pz} \cos\theta_A$

$$V_B = r.\hat{\mathbf{p}}_\mathbf{B} = V_{px} \sin\theta_B - V_{pz} \cos\theta_B$$

where $\hat{\mathbf{p}}_\mathbf{A}$ is the unit vector along PA, and $\hat{\mathbf{p}}_\mathbf{B}$ is the unit vector along PB and V_A, V_B are the

Doppler velocities measured by lidars A,B respectively.

Hence $V_{px} = -[V_A \cos\theta_B - V_B \cos\theta_A]/\sin(\theta_A + \theta_B)$

$$V_{pz} = -[V_A \sin\theta_B + V_B \sin\theta_A]/\sin(\theta_A + \theta_B)$$

Thus provided that $\sin(\theta_A + \theta_B) \neq 0$, one can in principle, obtain two components of the velocity at any point P in the vertical plane. These are the "along-track" and the vertical components . There is no information at all about the cross-track component. However, this can be estimated if a VAD scan is performed immediately afterwards.

3. Scans of points vertically above the circle with line joining lidars as a diameter

Lidars are at A,B, distance 2R apart.
N is a point on circle with diameter AB : OA=OB=ON=R.
P is a point on the vertical through N; PN=h
Angle BON = ϕ

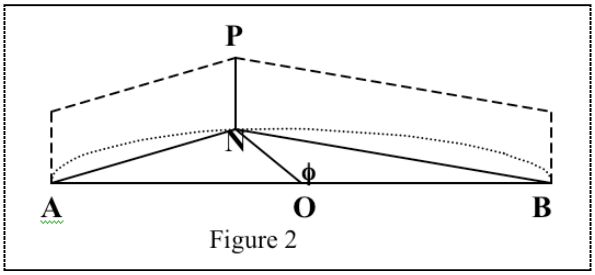

Figure 2

$$\hat{\mathbf{p}}_{\mathbf{A}} = \frac{1}{\sqrt{h^2 + 4R^2\cos^2(\phi/2)}}(-R - R\cos\phi, -R\sin\phi, -h)$$

$$\hat{\mathbf{p}}_{\mathbf{B}} = \frac{1}{\sqrt{h^2 + 4R^2\sin^2(\phi/2)}}(+R - R\cos\phi, -R\sin\phi, -h)$$

If $\mathbf{V}_p = V_{px}\hat{\mathbf{x}} + V_{py}\hat{\mathbf{y}} + V_{pz}\hat{\mathbf{z}}$

$$\sqrt{h^2 + 4R^2\cos^2(\phi/2)} \quad \mathbf{r}.\hat{\mathbf{p}}_{\mathbf{A}} = ((-R - R\cos\phi)V_{px} - R\sin\phi V_{py} - hV_{pz})$$

$$\sqrt{h^2 + 4R^2\sin^2(\phi/2)} \quad \mathbf{r}.\hat{\mathbf{p}}_{\mathbf{B}} = ((R - R\cos\phi)V_{px} - R\sin\phi V_{py} - hV_{pz})$$

Hence $V_{px} = \frac{1}{2R}\left[\sqrt{h^2 + 4R^2\sin^2(\phi/2)}\, V_B - \sqrt{h^2 + 4R^2\cos^2(\phi/2)}\, V_A\right]$

where V_B and V_A are Doppler radial velocities measured by *B* and *A* respectively.

Also

$$-\cos\phi\, V_{px} - \sin\phi V_{py} - \frac{h}{R}V_{pz} = \frac{1}{2R}\left[\sqrt{h^2 + 4R^2\sin^2(\phi/2)}\, V_B + \sqrt{h^2 + 4R^2\cos^2(\phi/2)}\, V_A\right]$$

Special Cases

If $\phi = 90°$ $\qquad V_{px} = (V_B - V_A)\frac{\sqrt{h^2 + 2R^2}}{2R}$

$$V_{py} + \frac{h}{R} V_{pz} = -(V_B + V_A) \frac{\sqrt{h^2 + 2R^2}}{2R}$$

If $\phi = 0°$ $\qquad V_{px} = \frac{h}{2R} V_B - \frac{\sqrt{h^2 + 4R^2}}{2R} V_A$

$$-V_{px} - \frac{h}{R} V_{pz} = \frac{h}{2R} V_B + \frac{\sqrt{h^2 + 4R^2}}{2R} V_A$$

$$\Rightarrow \qquad V_{pz} = -V_B$$

$$V_{px} = \frac{h}{2R} V_B - \frac{\sqrt{h^2 + 4R^2}}{2R} V_A$$

Thus, in this scan pattern, the along track velocity component can be extracted unambiguously. In the special case of one lidar pointing vertically, the vertical component can also be extracted. **For low elevation scans**, where $h << R$ we neglect terms in $\frac{h}{R}$ and

$$V_{px} = \sin(\phi/2) V_B - \cos(\phi/2) V_A$$

$$-\cos\phi V_{px} - \sin\phi V_{py} = \sin(\phi/2) V_B + \cos(\phi/2) V_A$$

$$\therefore 2\sin^2(\phi/2) V_{px} - 2\sin(\phi/2)\cos(\phi/2) V_{py} = 2\sin(\phi/2) V_B$$

$$\Rightarrow \sin(\phi/2) V_{px} - \cos(\phi/2) V_{py} = V_B$$

$$\therefore \cos(\phi/2) V_{py} = (\sin^2(\phi/2) - 1) V_B - \sin(\phi/2)\cos(\phi/2) V_A$$

$$\Rightarrow V_{py} = -\cos(\phi/2) V_B - \sin(\phi/2) V_A$$

4 Hemi-spherical scans

Here we consider scans of points on the hemi-sphere with centre point of two lidars as the centre. A general point on the hemi-sphere P is given by

$$\underline{P} = R(\sin\theta\cos\phi, \sin\theta\sin\phi, \cos\theta)$$

We take azimuth ϕ anti-clockwise from OB. $\theta = 90 - \text{elev}$ where elev = elevation angle.

We have $\mathbf{r}.\hat{\mathbf{p}}_{\mathbf{A}} = V_{px}[-1 - \sin\theta\cos\phi] + V_{py}[-\sin\theta\sin\phi] + V_{pz}[-\cos\theta]$

$$\mathbf{V}.\hat{\mathbf{p}}_{\mathbf{B}} = V_{px}[1 - \sin\theta\cos\phi] + V_{py}[-\sin\theta\sin\phi] + V_{pz}[-\cos\theta]$$

Hence $\mathbf{r}.(\hat{\mathbf{p}}_{\mathbf{A}} - \hat{\mathbf{p}}_{\mathbf{B}}) = V_A - V_B = -2V_{px}$

$$\mathbf{r}.[\hat{\mathbf{p}}_{\mathbf{A}} + \hat{\mathbf{p}}_{\mathbf{B}}] = -2V_{py}\sin\theta\sin\phi - 2V_{pz}\cos\theta$$

$$\Rightarrow V_{px} = -\frac{1}{2}[V_A - V_B]$$

Here only the along-track component of the wind can be derived unambiguously.

10 ACKNOWLEDGEMENTS

This work was funded by HM Treasury under the Invest to Save Budget. Department for Environment, Food and Rural Affairs (DEFRA) acted on behalf of HM Treasury. QinetiQ work described herein was supported under Contract Number CU016-0000014438 and this support is acknowledged.

The authors also acknowledge assistance from members of the Met Office for the meteorological data herein. In particular D J Thomson who advised on the ADMS Boundary Layer scheme and D B Ryall for the NAME data retrievals.

11 DISCLAIMER

The authors of this report are employed by QinetiQ, the Met Office, Salford University and Essex University. The work reported herein was carried out under a Contract CU016-0000014438 Version 1.0 placed on 26 October 2001 between QinetiQ and the Secretary of State for Environment, Food and Rural Affairs. Any views expressed are not necessarily those of the Secretary of State for Environment, Food and Rural Affairs.

12 DISTRIBUTION LIST

Copy No.	Name	Address
1-4	Dr Janet Dixon	DEFRA
5	Prof D V Willetts	PD315, QinetiQ Malvern
6	Dr G N Pearson	PD313, QinetiQ Malvern
7	Dr R I Young	PD115, QinetiQ Malvern
8-11	Dr D Middleton	Met Office
12	Prof C Collier	Salford University
13	Dr F Davies	Salford University
14	Dr K Bozier	Salford University
15	Prof A Holt	Essex University
16	Dr G Upton	Essex University
17	Project File	PD115, QinetiQ Malvern
18-23	Spares	PD115, QinetiQ Malvern